# Bootstrap Approximation for the Exchange-Correlation Kernel of Time-Dependent Density-Functional Theory

S. Sharma,* J. K. Dewhurst, A. Sanna, and E. K. U. Gross
*Max-Planck-Institut für Mikrostrukturphysik, Weinberg 2, D-06120 Halle, Germany*
(Received 1 July 2011; published 25 October 2011)

A new parameter-free approximation for the exchange-correlation kernel $f_{xc}$ of time-dependent density-functional theory is proposed. This kernel is expressed as an algorithm in which the exact Dyson equation for the response, as well as an approximate expression for $f_{xc}$ in terms of the dielectric function, are solved together self-consistently, leading to a simple parameter-free kernel. We apply this to the calculation of optical spectra for various small band gap (Ge, Si, GaAs, AlN, $TiO_2$, SiC), large band gap (C, LiF, Ar, Ne), and magnetic (NiO) insulators. The calculated spectra are in very good agreement with the experiment for this diverse set of materials, highlighting the universal applicability of the new kernel.

DOI: 10.1103/PhysRevLett.107.186401 PACS numbers: 71.15.Qe, 71.10.−w, 71.15.Mb, 71.35.−y

The *ab initio* calculation of optical absorption spectra of nanostructures and solids is a formidable task. The current state-of-the-art is based on many-body perturbation theory. A typical calculation involves two distinct steps: First, the quasiparticle spectral density function is calculated using the *GW* approximation, yielding accurate electron removal and addition energies, and is therefore a good prediction for the fundamental gap. In the second step, the Bethe-Salpeter equation (BSE) is solved using the one-body Green's function obtained in the *GW* step. Resonances, corresponding to bound electron-hole pairs called excitons, which have energies inside the gap, can then appear in the spectrum. The two-step procedure described above is a well-established method for yielding macroscopic dielectric tensors which are generally in good agreement with the experiment [1–6]. Unfortunately, solving the BSE involves diagonalizing a large matrix which couples different Bloch state $k$ points. As a consequence, the method is computationally expensive.

Time-dependent density-functional theory (TDDFT) [7], which extends density-functional theory into the time domain, is another method able, in principle, to determine neutral excitations of a system. Although formally exact, the predictions of TDDFT are only as good as the approximation of the exchange-correlation (xc) kernel: $f_{xc}(\mathbf{r}, \mathbf{r}', t - t') \equiv \delta v_{xc}(\mathbf{r}, t)/\delta\rho(\mathbf{r}', t')$, where $v_{xc}$ is the time-dependent exchange-correlation potential and $\rho$ is the time-dependent density. There are several such approximate kernels in existence, the earliest of which is the adiabatic local density approximation (ALDA) [8], where $v_{xc}(\mathbf{r}, t)$ is determined from the usual ground-state local density approximation (LDA), calculated instantaneously for $\rho(\mathbf{r}, t)$. In practice, however, the macroscopic dielectric function calculated using this kernel has two well-known deficiencies: the quasiparticle gap is too small, and the physics of the bound electron-hole pair is totally missing—in fact, ALDA does not improve on the results obtained within the random phase approximation (RPA) which corresponds to the trivial kernel $f_{xc} = 0$ [9]. In the present work, we concentrate on the second of these problems, namely, the missing excitonic peak in the spectrum. There have been previous attempts to solve this problem [10], and there exist kernels which correctly reproduce the peaks in the optical spectrum associated with bound excitons. The nanoquanta kernel by Sottile *et al.* [11], derived from the four-point Bethe-Salpeter kernel, is very accurate but has the drawback of being nearly as computationally demanding as solving the BSE itself. The long-range correction (LRC) kernel [12,13] has a particularly simple form in reciprocal space, $f_{xc} = -\alpha/q^2$, which limits its computational cost. This kernel produces the desired excitonic peak but depends on the choice of the parameter $\alpha$, which turns out to be strongly material-dependent [14], thereby limiting the predictiveness of this approximation. In the present Letter, we propose a new parameter-free approximation for $f_{xc}$ and demonstrate that this kernel gives accurate results with the computational cost of ALDA.

The exact relationship between the dielectric function $\varepsilon$ and the kernel $f_{xc}$ for a periodic solid can be written as

$$\begin{aligned}\varepsilon^{-1}(\mathbf{q}, \omega) &= 1 + v(\mathbf{q})\chi(\mathbf{q}, \omega) \\ &= 1 + \chi_0(\mathbf{q}, \omega)v(\mathbf{q})\{1 - [v(\mathbf{q}) \\ &\quad + f_{xc}(\mathbf{q}, \omega)]\chi_0(\mathbf{q}, \omega)\}^{-1}, \end{aligned} \tag{1}$$

where $v$ is the bare Coulomb potential, $\chi$ is the full response function, and $\chi_0$ is the response function of the noninteracting Kohn-Sham system. All these quantities are matrices in the basis of reciprocal lattice vectors $\mathbf{G}$. We approximate $f_{xc}(\mathbf{q}, \omega)$ by

$$f_{xc}^{\text{boot}}(\mathbf{q}, \omega) = -\frac{\varepsilon^{-1}(\mathbf{q}, \omega = 0)v(\mathbf{q})}{\varepsilon_0^{00}(\mathbf{q}, \omega = 0) - 1} = \frac{\varepsilon^{-1}(\mathbf{q}, \omega = 0)}{\chi_0^{00}(\mathbf{q}, \omega = 0)}, \tag{2}$$

where $\varepsilon_0(\mathbf{q}, \omega) \equiv 1 - v(\mathbf{q})\chi_0(\mathbf{q}, \omega)$ denotes the dielectric function in the RPA. The superscript 00 indicates that

 

only the $\mathbf{G} = \mathbf{G}' = 0$ component is used in the denominator. The approximate functional in Eq. (2) is designed in such a way that it satisfies two important requirements. (a) $f_{xc}$ has the exact long-wavelength behavior [1,15] $f_{xc}(\mathbf{q} \to 0) = \alpha_{xc}/q^2$. Satisfaction of this condition ensures that the dielectric function $\varepsilon(\mathbf{q} \to 0, \omega)$ may have a pole (i.e., a bound exciton) at some finite frequency, a feature that neither RPA nor ALDA allows. This immediately follows from the exact representation $\varepsilon \equiv 1 - v\chi_0/(1 - f_{xc}\chi_0)$ and from the fact that $\chi_0(\mathbf{q} \to 0) = x_0 q^2$. (b) In the $\omega \to 0$ limit, the form of $f_{xc}$ should yield static dielectric constants close to the RPA values, which are known to reproduce experiments reasonably well. Satisfaction of condition (b), for any functional satisfying (a), is a highly nontrivial requirement because RPA corresponds to $f_{xc} \equiv 0$. To demonstrate that the approximation (2) satisfies condition (b), we plug Eq. (2) into Eq. (1) and solve for $\varepsilon^{-1}(\omega = 0)$, ignoring, for simplicity, the matrix nature of $\chi_0$, $\varepsilon$, and $f_{xc}$. The resulting inverse dielectric constant $\varepsilon^{-1}(\omega = 0) = 1 - v\chi_0(\omega = 0)/2 - \sqrt{[v\chi_0(\omega = 0)]^2/4 - v\chi_0(\omega = 0)}$ is plotted in Fig. 1, and we find it is close to that obtained with the RPA.

We further note that, while Eq. (1) is exact, it is useful only when either $f_{xc}$ or $\varepsilon$ is given; if neither are available, then obviously it cannot be used as a generating equation for both quantities. With the addition of the approximation given by Eq. (2), however, both $f_{xc}$ and $\varepsilon$ can be determined from knowledge of $\chi_0$ exclusively. The *modus operandi* for doing so is to start by setting $f_{xc} = 0$ and then solving Eq. (1) to obtain $\varepsilon^{-1}$. This is then "bootstrapped" in Eq. (2) to find a new $f_{xc}$, and the procedure repeated until self-consistency between the two equations at $\omega = 0$ is achieved. This form of the kernel has two major advantages: the computation cost is minimal, as the most expensive part is the calculation of $\chi_0$, which needs to be calculated only once [16], and, most importantly, no system-dependent external parameter is required.

The $\chi_0$ in Eqs. (1) and (2) are, in practice, calculated using an approximate ground-state xc functional, such as the LDA. To overcome the shortcomings of such an approximation, we further replace the $\chi_0$ by a model response function $\chi_m$ coming either from scissors-corrected LDA or from $GW$ or from LDA + $U$ [17]. This has the advantage that $\chi_m$, and consequently $\chi$, has the correct gap to begin with. From the formal point of view, this replacement amounts to approximating the TDDFT kernel by

$$f_{xc}^{appr}(\mathbf{q}, \omega) = \frac{1}{\chi_0(\mathbf{q}, \omega)} - \frac{1}{\chi_m(\mathbf{q}, \omega)} + f_{xc}^{boot}(\mathbf{q}). \quad (3)$$

Using the method outlined above, optical spectra for various extended systems [18] were calculated using the full-potential linearized augmented plane wave method [19], implemented within the ELK code [20]. Except for the case of solid Ar, a shifted $k$-point mesh of $15 \times 15 \times 15$ is used to ensure convergence [21]. In the case of solid Ar, a shifted mesh of $25 \times 25 \times 25$ $k$ points was required for convergence of the optical spectrum. All the calculations were performed by scissor shifting the ground-state Kohn-Sham eigenvalues.

Presented in Fig. 2 are the results for some small (Ge ~ 0.67 eV) to medium (diamond ~5.47 eV) band gap semiconductors. For comparison, experimental data, as well as the RPA spectra, are also plotted. The experimental data clearly show that all these materials have weakly bound excitons, leading to a small shifting of the spectral weight to lower energies, compared to RPA. The results from TDDFT with the new kernel exactly follow this trend and are in excellent overall agreement with the experiment.

For Ge, the TDDFT results are only slightly different from the RPA values which themselves are in agreement with experiment. It is clear that, for Ge, the RPA is enough and $f_{xc}$ does not significantly improve on the result. This is in complete contrast to the spectrum of Si, where the spectral weight is redistributed and, corresponding to experiment, the TDDFT results show an enhanced $E_1$ peak. The height of the $E_2$ peak remains marginally overestimated by TDDFT. This overestimation is not particular to the present approximation for $f_{xc}$; it is also a feature of the BSE-derived kernel [11]. The dielectric function for GaAs

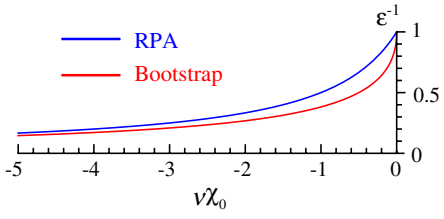


FIG. 1 (color online). $\varepsilon^{-1}$ as a function of $v\chi_0$.

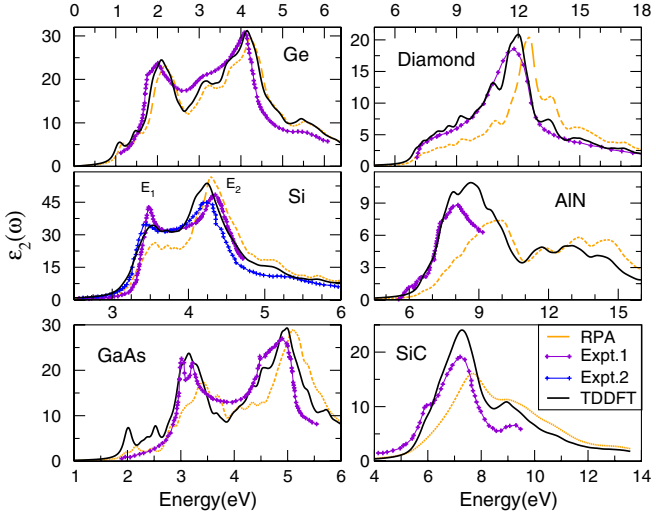


FIG. 2 (color online). Imaginary part of the dielectric tensor ($\varepsilon_2$) as a function [21] of photon energy (in eV). Experimental data are taken from the following sources: Ge from [22], Si from [23] and [22], GaAs from [24], diamond from [25], AlN from [26], and SiC from [27].

is also in very good agreement with the experiment—subtle features like the kink at 4.25 eV are well-captured by the bootstrap procedure.

The second column of Fig. 2 contains results for medium band gap insulators. In all these materials, a significant redistribution of the spectral weight to lower photon energies is observed. For diamond, the bootstrap procedure correctly leads to an enhancement of the shoulder at low photon energies. The position of the main peak around 12 eV is shifted to lower energies, and the whole spectrum is in near-perfect agreement with the experiment. AlN is a particularly interesting case—TDDFT shifts the spectral weight to lower energies, and, although the height of the peak is too large, the agreement with the experiment is considerably better than that obtained by the equivalent BSE calculation [28–30]. For SiC, the results show an improvement over the RPA spectrum, but the height of the main peak, as well as the shoulder at 9 eV, are overestimated. This trend is also observed in previous BSE results [31].

A stringent test for any approximate xc kernel is in its ability to treat materials with strongly bound excitons. In these cases, a new resonant peak appears in the band gap itself and represents the bound state of an electron-hole pair. Perhaps the most studied test case for this phenomenon is the ionic solid LiF. Other excitonic materials which have also attracted attention and are considered particularly difficult to treat are the noble gas solids. Plotted in the first column of Fig. 3 are the results for three materials of this class: LiF, solid Ar, and Ne. What is immediately clear is that the bootstrap procedure, which gave only a slight shift of spectral weight for Ge, now gives rise to an entirely new bound excitonic peak inside the gap in all three cases. The location of the peak, which corresponds to the excitonic binding energy, is also very well-reproduced for all these materials.

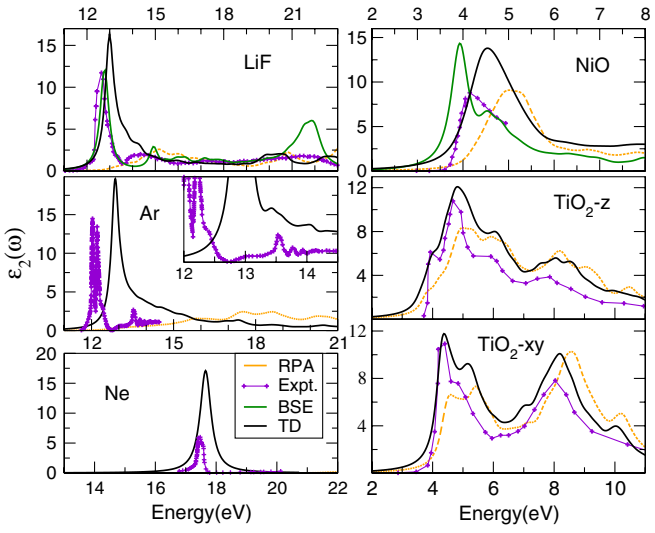


FIG. 3 (color online). Imaginary part of the dielectric tensor ($\varepsilon_2$) as a function [21] of photon energy (in eV). Experimental data are taken from the following sources: LiF from [32], Ar and Ne from [33], NiO from [34], and $TiO_2$ from [35]. In the inset, a smaller broadening is used to better resolve the peaks [21].

Despite a good overall agreement, we find that, for LiF, the main peak at 12.5 eV is overestimated, and the peak at 14.3 eV appears as a hump in the TDDFT results. Nevertheless, it is encouraging to note that the BSE spectrum, as well that obtained using the BSE-derived kernel [36], includes a spurious peak at around 21 eV which is absent in the present calculations. Noble gas solids have very weak band dispersion and polarizability, which results in very strongly bound electron-hole pairs. In the case of solid Ar, one can observe a strongly localized Frenkel exciton [37] at about 12 eV and a Wannier exciton at about 14 eV. This physics is totally missing within the RPA. Remarkably, though, the bootstrap procedure captures both these excitons, although the Wannier exciton is suppressed (see inset). Exactly like in BSE and LRC calculations [37], the Frenkel exciton is underbound by 0.7 eV. Ne has a strongly bound Frenkel exciton, and the present calculations capture the corresponding excitonic peak. Similar to the BSE results [38], the height of this peak is overestimated by the present TDDFT calculations.

The second column of Fig. 3 consists of some special cases—NiO has an antiferromagnetic ground state, and the LDA + $U$ method is needed to obtain a physically reasonable band structure for this material. This material provides the bootstrap technique with a test of its validity for magnetic materials and also with a check of its performance when the scissors-corrected LDA is replaced by LDA + $U$, where $U$ is chosen to reproduce the experimental gap. It is clear from Fig. 3 that the bootstrap method leads once again to the correct excitonic binding energy. The experimental data for NiO are rather old and substantially broadened [34], and, assuming the veracity of these data, both TDDFT and BSE [39] overestimate the peak height. It is worth noting that the BSE spectrum is redshifted relative to the experiment and the TDDFT spectrum. Results for the anatase phase of $TiO_2$ are also presented in Fig. 3. This material is important for its industrial use in photovoltaics and has been well-characterized using the BSE and $GW$ method [40,41], as well as the experiment [35]. $TiO_2$ is a useful test for the bootstrap method due to its noncubic unit cell, which leads to directional anisotropy in the optical spectrum. As can be seen in Fig. 3, the bootstrap method captures this anisotropy very well indeed. Even subtle features, like the small shoulder at ~4 eV in the out-of-plane dielectric function, which is missing in the in-plane case, are well-reproduced. We find that our peak heights, like BSE results [40], are slightly overestimated.

It is also interesting to compare the real part of the dielectric function with available experimental data. Results for Si, GaAs, and diamond are presented in Fig. 4. In all three cases, TDDFT results are in excellent

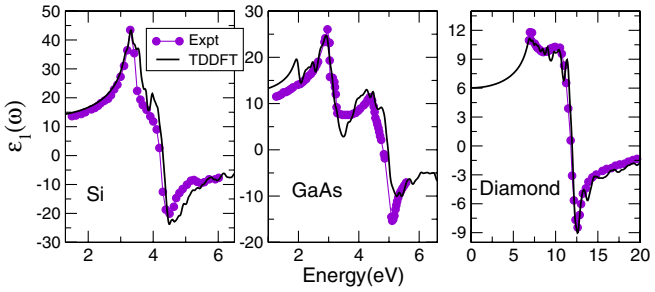


FIG. 4 (color online). Real part of the dielectric tensor ($\varepsilon_1$) as a function of photon energy (in eV) for Si, GaAs, and diamond.

agreement with the experimental data. We note that, in the low-frequency regime (below 2 eV), the TDDFT results for GaAs deviate from experiments in exactly the same manner as found for the LRC kernel [31].

We further note that $f_{xc}$ in Eq. (2) is related to the two existing TDDFT kernels which capture the excitonic physics. In particular, it corresponds to the LRC kernel when $\alpha = 4\pi\varepsilon^{-1}/(\varepsilon_0 - 1)$, and $\varepsilon$ is determined self-consistently. Also, like for the LRC kernel, the $\mathbf{G} = \mathbf{G}' = 0$ part of $f_{xc}$ is by far the most important contribution. Comparing our kernel to the BSE-derived approximation, in both cases, the $f_{xc}$ is proportional to the screened Coulomb matrix elements $\varepsilon^{-1}v$. Choosing $f_{xc}$ to be proportional to $\varepsilon^{-1}v$ was also exploited by Turkowski *et al.* {see Eqs. (1) and (15) of Ref. [42]}. There remain several interesting aspects of the bootstrap method to be explored in the future. (1) The first is determination of the energy loss spectrum for finite $\mathbf{q}$. Since ALDA is known to give accurate results for finite $\mathbf{q}$, it is also possible to combine the bootstrap kernel in the $q \to 0$ limit with the ALDA for large values of $\mathbf{q}$, e.g., using the additive form $f_{xc}^{Comb} = f_{xc}^{boot}(\mathbf{q} \to 0) + f_{xc}^{ALDA}$ which automatically ensures that $f_{xc}^{boot}$ dominates for small $\mathbf{q}$ while $f_{xc}^{ALDA}$ dominates for larger $\mathbf{q}$. (2) Performance of the bootstrap approximation for two-dimensional systems, like graphene sheets or nanotubes where excitonic effects are particularly strong and (3) performance for excitonic spectra of molecular aggregates are also interesting aspects.

Thus, we have demonstrated that the bootstrap procedure gives a parameter-free TDDFT kernel which yields very accurate optical spectra. The same functional which produces a small shift, relative to the RPA, in the absorption edge of Ge also generates an entirely new excitonic peak within the bandgap of LiF, Ar, and Ne. This indicates that the bootstrap kernel has wide applicability for very small computation effort.

*sharma@mpi-halle.mpg.de

[1] G. Onida *et al.*, Rev. Mod. Phys. **74**, 601 (2002).
[2] G. Onida *et al.*, Phys. Rev. Lett. **75**, 818 (1995).
[3] S. Albrecht *et al.*, Phys. Rev. Lett. **80**, 4510 (1998).
[4] L. X. Benedict, E. L. Shirley, and R. B. Bohn, Phys. Rev. B **57**, R9385 (1998).
[5] M. Rohlfing and S. G. Louie, Phys. Rev. Lett. **81**, 2312 (1998).
[6] A. Marini *et al.*, Comput. Phys. Commun. **180**, 1392 (2009).
[7] E. Runge and E. K. U. Gross, Phys. Rev. Lett. **52**, 997 (1984).
[8] E. K. U. Gross, F. J. Dobson, and M. Petersilka, Top. Curr. Chem. **181**, 81 (1996) and references therein.
[9] V. I. Gavrilenko and F. Bechstedt, Phys. Rev. B **55**, 4343 (1997).
[10] S. Botti *et al.*, Rep. Prog. Phys. **70**, 357 (2007).
[11] F. Sottile, V. Olevano, and L. Reining, Phys. Rev. Lett. **91**, 056402 (2003).
[12] L. Reining *et al.*, Phys. Rev. Lett. **88**, 066404 (2002).
[13] S. Botti *et al.*, Phys. Rev. B **72**, 125203 (2005).
[14] The value of $\alpha$ required to reproduce the bootstrap spectra (in Ha): Ge 0.036, Si 0.085, GaAs 0.1, AlN 0.915, SiC 0.327, diamond 0.487, LiF 6.65, Ar 10.15, Ne 53.735, NiO 0.53, and TiO2 0.346.
[15] P. Ghosez, X. Gonze, and R. W. Godby, Phys. Rev. B **56**, 12811 (1997).
[16] For a typical case of LiF, with 64 $\mathbf{k}$ points, $\chi_0$ required 214 s to calculate and the bootstrap procedure a further 1 s on 4 processors. The BSE calculations required 1100 s.
[17] See Supplemental Material at http://link.aps.org/supplemental/10.1103/PhysRevLett.107.186401 to look at the effect of the scissors correction on the TDDFT spectra.
[18] The following experimental lattice parameters (in a.u.) were used: Ge 10.69; Si 10.26; GaAs 10.6870; AlN 8.2760; SiC 8.2386; diamond 6.7274; LiF 7.608 04; Ar 10.030; Ne 8.440; NiO 7.893 389; and TiO2 a = 7.1511, c = 8.9899.
[19] D. J. Singh, *Planewaves, Pseudopotentials, and the LAPW Method* (Kluwer, Boston, 1994).
[20] http://elk.sourceforge.net, 2004.
[21] The calculated spectra are broadened by (in eV): Ge 0.1, Si 0.05, GaAs 0.1, AlN 0.2, SiC 0.23, diamond 0.22, LiF 0.16, Ar 0.2 (0.1 for inset), Ne 0.2, NiO 0.2, and TiO2 0.16.
[22] D. E. Aspnes and A. A. Studna, Phys. Rev. B **27**, 985 (1983).
[23] P. Lautenschlager *et al.*, Phys. Rev. B **36**, 4821 (1987).
[24] P. Lautenschlager *et al.*, Phys. Rev. B **35**, 9174 (1987).
[25] D. Edwards and H. Philipp, *Handbook of Optical Constants of Solids*, edited by E. D. Palik (Academic, Orlando, 1985).
[26] V. Cimalla *et al.*, Phys. Status Solidi C **2**, 2199 (2005).
[27] S. Logothetidis and J. Petalas, J. Appl. Phys. **80**, 1768 (1996).
[28] F. Bechstedt *et al.*, Phys. Rev. B **72**, 245114 (2005).
[29] P. H. Hahn *et al.*, Phys. Status Solidi B **242**, 2720 (2005).
[30] R. Laskowski and N. E. Christensen, Phys. Status Solidi B **244**, 17 (2007).
[31] S. Botti *et al.*, Phys. Rev. B **69**, 155112 (2004).
[32] D. Roessler and W. Walker, J. Opt. Soc. Am. **57**, 835 (1967).
[33] B. Sonntag, in *Rare Gas Solids*, edited by M. L. Klein and J. A. Venables (Academic, London, 1976), Vol. II, p. 10211117.

[34] R. J. Powell and W. E. Spicer, Phys. Rev. B **2**, 2182 (1970).
[35] N. Hosaka *et al.*, J. Phys. Soc. Jpn. **66**, 877 (1997).
[36] A. Marini, R. DelSole, and A. Rubio, Phys. Rev. Lett. **91**, 256402 (2003).
[37] F. Sottile *et al.*, Phys. Rev. B **76**, R161103 (2007).
[38] S. Galamic-Mulaomerovic and C. H. Patterson, Phys. Rev. B **72**, 035127 (2005).
[39] C. Rödl, Elektronische und exzitonische Anregungen in magnetischen Isolatoren (2010), p. 74.
[40] H. M. Lawler *et al.*, Phys. Rev. B **78**, 205108 (2008).
[41] W. Kang and M. S. Hybertsen, Phys. Rev. B **82**, 085203 (2010).
[42] V. Turkowski, A. Leonardo, and C. A. Ullrich, Phys. Rev. B **79**, 233201 (2009).